I-U dependence of $TlInX_2$ (X=Se,Te) single crystals: The Ohmic and S-type regions

M. Hanias, A. N. Anagnostopoulos, K. Kambas, and J. Spyridelis
Department of Physics, Aristoteles University of Thessaloniki, Solid State Section 313-1, 540 06 Thessaloniki, Greece
(Received 29 May 1990)

Electrical conductivity measurements were performed on $TlInSe_2$ and $TlInTe_2$ single crystals. The corresponding current-voltage (I-U) characteristics consist of two parts: An Ohmic part, at low current densities, and a nonlinear one of the S type, at moderate and higher current densities. In the latter part a well-formed negative-differential-resistance (NDR) region appears. Acceptor levels and their concentrations were determined from $\ln p$ versus $10^3/T$ curves measured in the Ohmic region of the corresponding I-U curves. The nonlinear behavior of the I-U curves was studied at different ambient temperatures; the sample temperature and the threshold voltage of the NDR region were examined as a function of the current density and the ambient temperature, respectively.

I. INTRODUCTION

The $TlInX_2$ (X=Se,Te) compounds are p-type semiconductors[1-3] with indirect energy gaps[4-6] and structures that can be described as $[In^{3+}X^{2-}{}_2]^-$ chains, extending along the crystallographic c axis of the materials.[7,8] Such negatively charged chains are bonded together by Tl^+ ions, forming a tetragonal lattice of group symmetry D^{18}_{4h}-$I4/mcm$.[9]

These compounds exhibit, in their electrical behavior, many nonlinear effects, such as S-type characteristics with voltage oscillations in the negative resistance region[6] and switching and memory effects registered both on pure and Li-intercalated crystals.[10,11]

Negative differential resistance (NDR) and electrical switching effects attracted the interest of many researchers[12] in the case of the chalcogenide glasses. This is due to possible technological applications such as switching and memory devices, oscillators, thermistors, etc. and also to the possibility of theoretical research on them such as bifurcation analysis; for the same reasons we think that a more detailed study of the electrical properties of the $TlInX_2$ (X=Se,Te) is necessary.[13] In the present work, we report on the acceptor levels regulating the electrical conductivity in the linear region of the corresponding I-U characteristics, as well as the influence of current density and temperature on the NDR regions.

II. EXPERIMENT

Electrical measurements were performed on both $TlInSe_2$ and $TlInTe_2$. The electrodes were made by evaporated In, which proved to form Ohmic contacts of low resistivity with these materials.[2,3,6] A four-contact geometry was used. A current flow along the c axis of the samples was ensured by a pair of contacts deposited on the two opposite surfaces of the rectangular-shaped samples.

Current-voltage (I-U) characteristics of the samples were measured in the temperature range 100–350 K. From now on these ambient temperatures will be denoted as T_0. The sample temperature T was always monitored at every point of the measured I-U characteristics. Typical characteristics measured for $TlInSe_2$ and $TlInTe_2$ are shown in Figs. 1 and 2, respectively. It is evident that two regions are present in the I-U curves; an Ohmic one at lower current densities and a nonlinear one, of S type, at moderate and higher current density values.

III. RESULTS AND DISCUSSION

A. Ohmic region

In the Ohmic region of each characteristic, the conductivity σ was estimated. From the conductivity σ the free-hole concentration p can be deduced, provided the mobilities for both compounds are given.[14] The corresponding $\ln p$ versus $10^3/T_0$ curves (Arrhenius plots) are given in Figs. 3 and 4. On the other hand, the electrical-

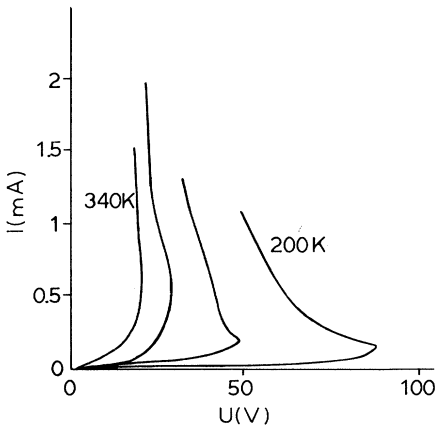

FIG. 1. Current-voltage (I-U) characteristics measured at different temperatures in $TlInSe_2$. The Ohmic and NDR regions are apparent in these curves.

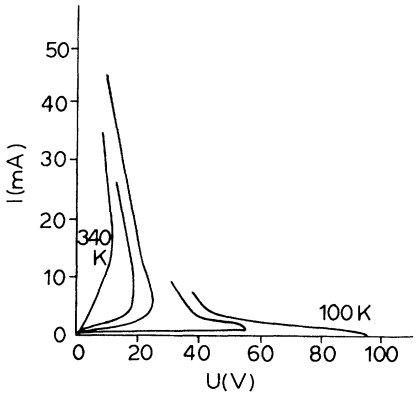

FIG. 2. Current-voltage (I-U) characteristics measured at different temperatures in $TlInTe_2$. The Ohmic and NDR regions are also apparent in these curves.

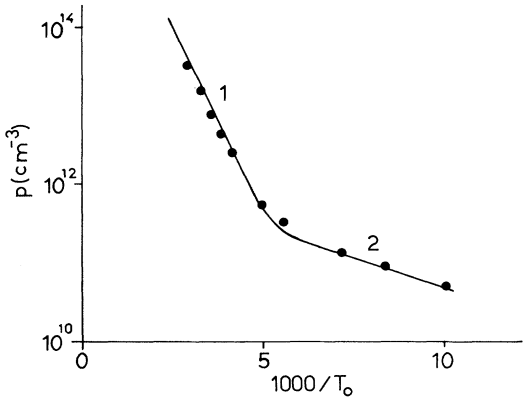

FIG. 4. The p vs $10^3/T_0$ plot for $TlInTe_2$, as measured in the Ohmic region of the corresponding I-U characteristics (solid circles) and as calculated using Eq. (2) with the following parameters: $E_{A1}-E_v=0.41$ eV and $A_1=4\times10^{14}$ cm^{-3}; $E_{A2}-E_v=0.030$ eV and $A_2=1\times10^{19}$ cm^{-3} (solid line).

neutrality condition applied in the present case gives[15]

$$p+C=A-A_p\ , \tag{1}$$

where C is the total concentration of compensating donor levels, A is the concentration of each acceptor level, and A_p is the concentration of each acceptor level occupied by holes.

Equation (1) can be transformed into the following:

$$10^3/T_0=-\frac{10^3k_B}{E_A-E_v}[\ln p+\ln(p+C)-\ln(A-C-p)-\ln N_v] \tag{2}$$

if the relations

$$p=N_v e^{-(E_F-E_v)/k_BT_0}\ , \tag{3}$$

$$A_p=A\frac{p}{p+p_A}\ , \tag{4}$$

and[16]

$$p_A=N_v e^{-(E_A-E_v)/k_BT_0} \tag{5}$$

are taken into account,[15] where E_v is the upper valence-band edge, E_A is the energy position of the considered acceptor level, N_v is the effective density of states in the valence band, and E_F is the Fermi level for each case.

A differential evaluation of Eq. (2) leads to the following result:[17]

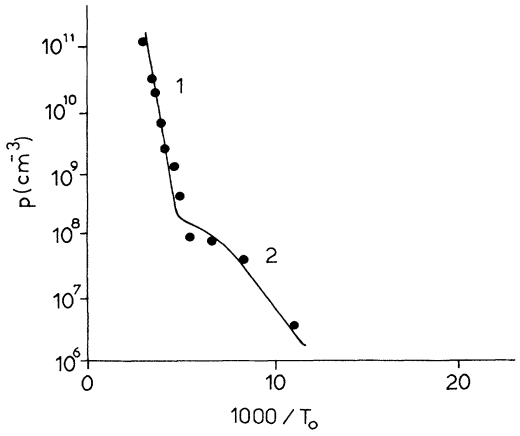

FIG. 3. The p vs $10^3/T_0$ plot for $TlInSe_2$, as measured in the Ohmic region of the corresponding I-U characteristics (solid circles), and as calculated using Eq. (2) with the following parameters; $E_{A1}-E_v=0.76$ eV and $A_1=3\times10^{14}$ cm^{-3}; $E_{A2}-E_v=0.088$ eV and $A_2=1\times10^{16}$ cm^{-3} (solid line).

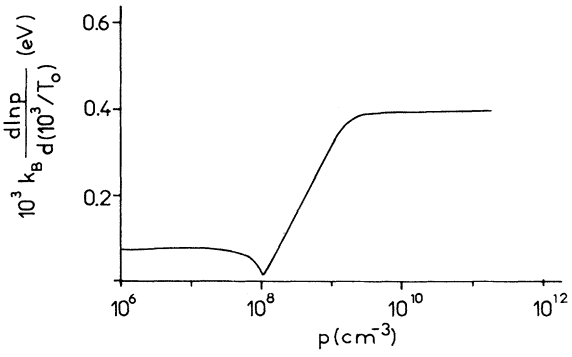

FIG. 5. The $d\ln p/d(10^3/T_0)$ vs p plot for $TlInSe_2$ as deduced from the corresponding experimental curve of Fig. 3; after that this curve was fitted with cubic splines. Note that the horizontal parts of the $d\ln p/d(10^3/T_0)$ vs p plot correspond to the energy levels: $(E_{A1}-E_v)/2=0.38$ eV and $(E_{A2}-E_v)=0.088$ eV.

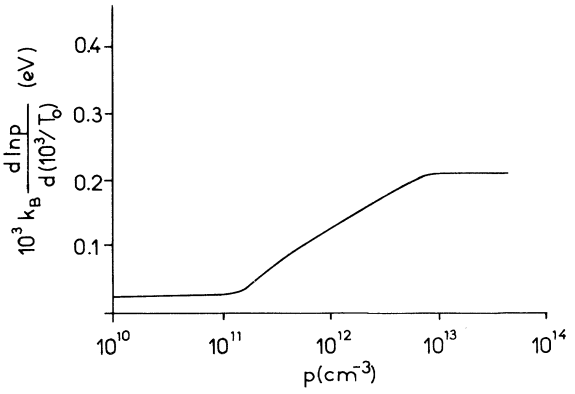

FIG. 6. The $d\ln p/d(10^3/T_0)$ vs p plot for $TlInTe_2$ as deduced from the corresponding experimental curve of Fig. 4; after that this curve was fitted with cubic splines. Note that the horizontal parts of the $d\ln p/d(10^3/T_0)$ vs p plot correspond to the energy levels; $(E_{A1}-E_v)/2=0.2$ eV and $(E_{A2}-E_v)=0.030$ eV.

$$\frac{d\ln p}{d(10^3/T_0)}=-\frac{(E_A-E_v)}{10^3 k_B}\left[1+\frac{Ap}{(p+C)(A-C-p)}\right]^{-1}. \tag{6}$$

Equation (6) can be further reduced in the particular cases of no compensation ($C=0$), weak compensation ($0\neq C \ll A$), and strong compensation ($C\rightarrow A$).

The experimental $\ln p$ versus $10^3/T_0$ characteristics (solid circles in Figs. 3 and 4) were fitted with cubic splines and subsequently their slope was calculated as a function of $\ln p$ (Figs. 5 and 6, respectively). These curves exhibit two horizontal parts, from which the energy levels of two acceptors in each compound were obtained. For the $TlInSe_2$ compound the acceptor levels were found to be 0.760 and 0.088 eV above E_v. The solid line in Fig. 3 represents a fitting of the experimental points with the help of Eq. (2) and using the previous estimated values of the two acceptor levels. The best fitting was obtained with concentrations 3×10^{14} cm^{-3} and 1×10^{16} cm^{-3}, respectively. The shallower level appears to be strongly compensated for. In the case of $TlInTe_2$ the acceptor levels were found to be 0.410 and 0.030 eV above E_v. The solid line in Fig. 4 represents a fitting of the experimental points with Eq. (2). For the above-mentioned values of the acceptor levels, the best values of concentrations are found to be 4×10^{14} and 1×10^{19} cm^{-3}, respectively. In this compound, the second acceptor also seems to be compensated for.

It should be mentioned here that although the plot in Fig. 4 is reminiscent of that due to the presence of bistable centers, the lack of any persistent photoconductivity characterizing such a level led us to the assumption of two distinct acceptor species.

B. Negative-differential-resistance (NDR) region

At moderate and higher current densities, the slope of the I-U curves becomes negative; the curves themselves show a strong nonlinear behavior. At even higher current densities the slope of the curves changes its sign once again, becoming positive, but its value is now much higher than that of the corresponding Ohmic region. The part of the I-U curves exhibiting the negative slope is usually called the negative differential resistance (NDR). Its width, slope, threshold voltage, and threshold current values (V_{th} and I_{th}) are the main characteristic features of this region.

If we are to decide about the mechanism governing the NDR region, we have to study the sample temperature distribution along this part of the I-U curve; i.e., we have to look for a change in the sample temperature T at every measured point of this region. Generally, two processes of quite different origin and character may govern the phenomenon: a pure electronic or an electrothermic one.

In electronic processes the high conductivity state connected with the appearance of the NDR region is due to an increase in the nonequilibrium majority carriers and/or to an increase in their mobility. This can be attributed to different mechanisms, such as the Gunn effect, tunneling effect, carriers injection, etc. Generally speaking, electronic processes are not connected directly with an increase in the sample temperature T in the NDR region.[18–20]

In electrothermal processes it is assumed that small local deviations from the homogeneous distribution of the imperfections lead to a higher current density in these regions. Such elevated current densities are usually accompanied by the formation of high-current-density filaments in the sample. Anyhow, according to the electrothermal model, it is assumed that a high-current-density filament exists in the sample. In this "channel" the elevated current density results in an increased power dissipation, leading to a joule heating. As the temperature increases, conductivity also increases, permitting a higher current to pass through. The steady state of this feed path is reached when the heat dissipation equals heat losses.[21]

Many mechanisms can be considered responsible for the onset of electrothermal processes. Impact ionization seems to be the most significant. In $TlInX_2$ (X=Se,Te), impact ionization leading to a NDR region in the I-U characteristic has already been mentioned in the literature.[10]

Hence, in cases of electrothermally generated NDR, we expect to measure a significant temperature elevation in the sample at the NDR region (Figs. 7 and 8), accompanied in general by a migration of its width and threshold voltage to higher values, with the ambient temperature T_0 (Refs. 18, 20, 22, and 23) being decreased.

In our case, all experimental data strongly support that the dominant process is of electrothermal origin. In this case,[22] the heat transport and electric current transport are described by the heat balance and Maxwell equations,

$$c_v\left[\frac{\partial T}{\partial t}\right]=\nabla\cdot(\kappa\nabla T)+\mathbf{j}\cdot\mathcal{E} \tag{7}$$

and

$$\mathbf{j}=\sigma\mathcal{E}\ , \tag{8}$$

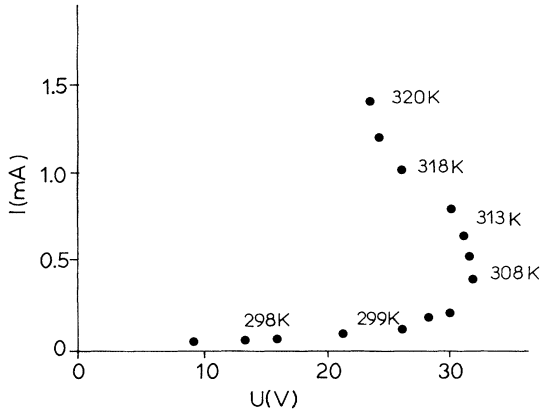

FIG. 7. The temperature elevation as estimated in the NDR region of the I-U curve (300 K) in $TlInSe_2$.

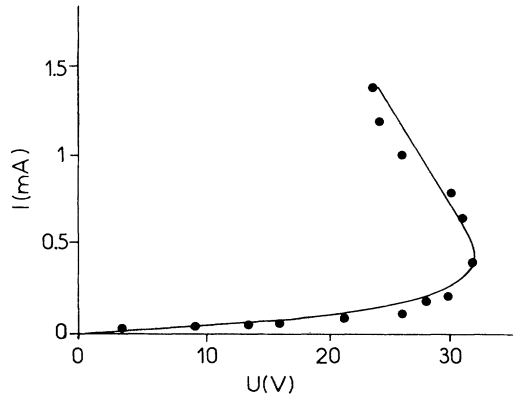

FIG. 9. The I-U curve as measured at 300 K in $TlInSe_2$ (solid circles) and as recreated with the help of Eqs. (9)–(11) (solid line).

respectively. c_v is the specific-heat coefficient, κ is the thermal conductivity coefficient, j is the current density, and $\mathcal{E}$ is the electric field strength.

Using the effective cooling term notation[19] to approximate axial heat losses and requiring radially independent solutions of the steady state $[(\partial T/\partial t)=0]$, the following relation is obtained:[21–23]

$$-\frac{8\kappa}{d^2}(T-T_0)+\sigma(T,\mathcal{E})\mathcal{E}^2=0 \tag{9}$$

while the current I and voltage drop U are given by

$$I=\pi R^2\sigma(T,\mathcal{E})\mathcal{E} \tag{10}$$

and

$$U=\mathcal{E}d\ , \tag{11}$$

where d is the distance between the electrodes.

If the sample temperature T at every point of the I-U characteristic is known, we can generate this curve using Eqs. (9)–(11). In Figs. 9 and 10, two typical examples of this procedure are shown. Measurements are denoted by solid circles, while the solid line represents solutions from the above-mentioned relations.

On the other hand, from a measured I-U characteristic, i.e., from the static resistance at every point of it, the temperature distribution at the various points of the I-U curve can be estimated. For this purpose the following relation is used:[24]

$$T=(E_A-E_v)T_0[(E_A-E_v)+k_BT_0\ln(R/R_{\rm th}-1)]^{-1}\ , \tag{12}$$

where $R_{\rm th}$ is the threshold resistance and R is the static resistance at every point of the I-U curve.

In Figs. 11 and 12 the sample temperature T is plotted as a function of the current flowing through it. Measurements are denoted with solid circles, while the solid lines are calculated from the corresponding I-U curves with use of Eq. (12) and the (E_A-E_u) values mentioned above.

As is evident from the experimental curves of Figs. 1

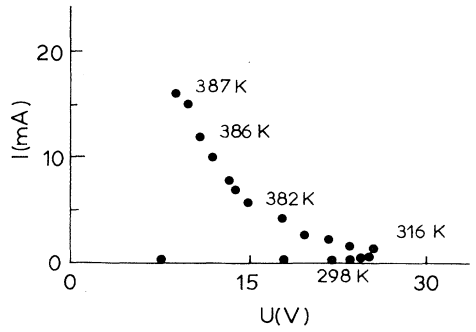

FIG. 8. The temperature elevation as estimated in the NDR region of the I-U curve (300 K) in $TlInTe_2$.

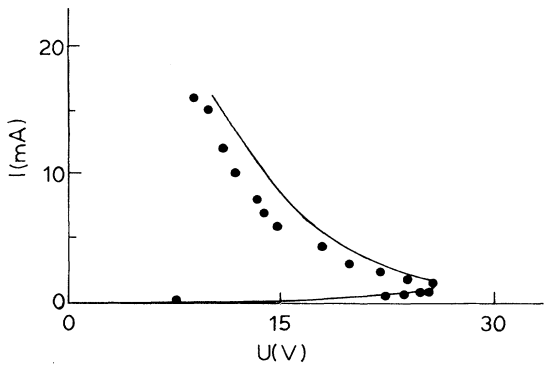

FIG. 10. The I-U curve as measured at 300 K in $TlInTe_2$ (solid circles) and as recreated with the help of Eqs. (9)–(11) (the solid line).

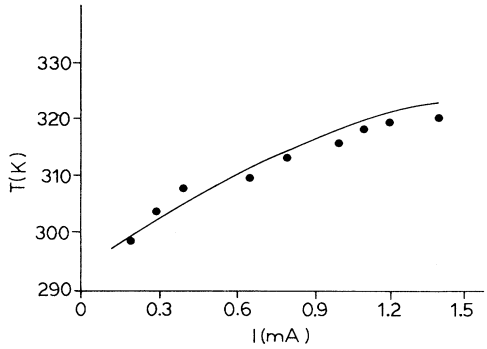

FIG. 11. The elevated sample temperature T vs the current I flowing through it in $TlInSe_2$ as measured in the sample (solid circles) and as computed using Eqs. (12) and (6) and the corresponding curve of Fig. 9 (solid line).

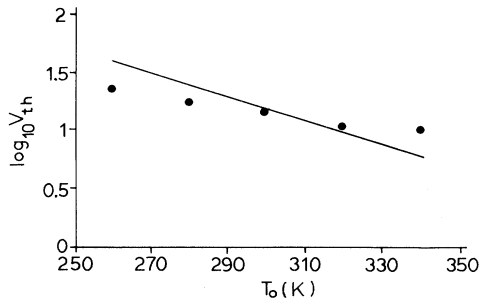

FIG. 13. The dependence of the threshold voltage V_{th} on the ambient temperature T_0 in the case of $TlInTe_2$; measurements are denoted by solid circles while the solid line represents calculations with relation (14a).

and 2, as well as predicted by the electrothermal model,[18–21,25] the ambient temperature T_0 greatly influences both the form of the I-U curves and the voltage V_{th} at which the NDR sets on.

As indicated in Refs. 18, 20, 22, and 23, the higher the ambient temperature, the weaker the appearance of the NDR region of the I-U characteristic. This is a reasonable consequence of the fact that at elevated ambient temperatures the inequality

$$\frac{8\kappa}{d^2}-\frac{\partial\sigma}{\partial t}\mathcal{E}^2+\sigma\frac{\mathcal{E}^2}{\kappa}L\left[\sigma+\frac{\partial\sigma}{\partial T}T\right]<0 \tag{13}$$

cannot hold simultaneously with Eq. (9),[22] where L is the Lorentz number.

The threshold voltage V_{th}, as indicated in the literature,[22] strongly depends on the distance d between the electrodes, leading to different expressions for V_{th} as $d\to\infty$ or $d\to 0$:

$$V_{th}=\begin{cases} d\left[\dfrac{8k_B\kappa}{\sigma_0(E_A-E_v)}\right]^{1/2}T_0\exp[(E_A-E_v)/2k_BT_0] & \text{for } d\to\infty \quad (14a)\\ 2d\mathcal{E}_0\left\{\ln\left[\left[\dfrac{8k_B\kappa}{(E_A-E_v)}\right]^{1/2}\dfrac{1}{2\sigma_0 d\mathcal{E}_0}\right]+\ln T_0+\dfrac{E_A-E_v}{2k_BT_0}\right\} & \text{for } d\to 0\ , \quad (14b)\end{cases}$$

where $\mathcal{E}_0=0.4(V_{th}/d)$ and σ_0 is the prefactor of the thermally activated conductivity $\sigma=\sigma_0\exp[(E_A-E_v)/k_BT]$.

For $TlInSe_2$, d was 0.6 mm, while for $TlInTe_2$, d was 4 mm. Therefore their behavior can be described only approximately by Eqs. (14a) and (14b). In Figs. 13 and 14 the corresponding measured V_{th} values, denoted by solid circles, are plotted as a function of the ambient temperature T_0, while solid lines represent corresponding curves

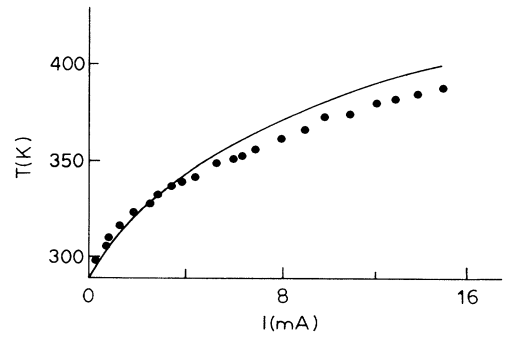

FIG. 12. The elevated sample temperature T vs the current I flowing through it in $TlInTe_2$ as measured in the sample (solid circles) and as computed using Eqs. (12) and (6) and the corresponding curve of Fig. 10 (solid line).

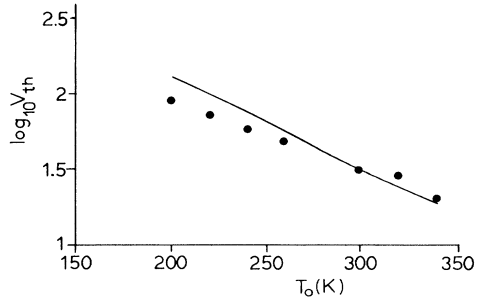

FIG. 14. The dependence of the threshold voltage V_{th} on the ambient temperature T_0 in the case of $TlInSe_2$; measurements are denoted by solid circles while the solid line represents calculations with relation (14b).

as predicted by Eqs. (14a) and (14b). As we can see from these curves, the agreement between theory and experiment is quite satisfactory.

IV. CONCLUSIONS

The ternary compounds $TlInX_2$ (X=Se,Te) show nonlinear electrical behavior at moderate and higher current densities.

Although the exact determination of the mechanism responsible for this behavior is not yet clear, it is certainly of electrothermal origin. This behavior, as mentioned in the literature,[10] shows all features of the impact ionization. Our experimental data suggesting its electrothermal origin support this point of view.

Applying the electrothermal model we tried to interpret the measured I-U curves, both qualitatively and quantitatively. Furthermore, the sample temperature distribution along the I-U curves as well as the dependence of V_{th} on d sufficiently corroborate this model.

[1]G. D. Guseinov, E. Mooser, E. M. Derimova, R. S. Gamidov, I. V. Alekseev, and M. Z. Ismailov, Phys. Status Solidi **34**, 33 (1969).

[2]G. D. Guseinov, V. A. Aliev, and E. F. Bagirzade, Phys. Status Solidi A **96**, K73 (1986).

[3]G. D. Guseinov, A. U. Malsagov, A. Kh. Matiev, S. Kh. Umarov, E. G. Abdulaev, and M. L. Shubnikov, Fiz. Tekh. Poluprovodn. **19**, 885 (1985) [Sov. Phys.—Semicond. **19**, 545 (1985)].

[4]K. R. Allakhverdiev, T. G. Mamedov, V. E. Steinschreiber, and I. K. Efendieva, Phys. Status Solidi B **127**, K55 (1985).

[5]A. E. Bakhyshov, M. F. Agaeva, and A. M. Darvish, Phys. Status Solidi B **91**, K31 (1979).

[6]M. Hanias, A. N. Anagnostopoulos, K. Kambas, and J. Spyridelis, Physica B **160**, 154 (1989).

[7]W. Henkel, H. D. Hochheimer, C. Carlone, A. Werner, S. Ves, and H. G. von Schnering, Phys. Rev. B **26**, 3211 (1982).

[8]G. D. Guseinov, G. G. Guseinov, E. M. Kerimova, M. Z. Ismailov, V. D. Rustamov, and L. A. Rzajeva, Mater. Res. Bull. **13**, 975 (1978).

[9]D. Müller, G. Eulenberger, and H. Hahn, J. Anorg. Allg. Chem. **398**, 207 (1973).

[10]A. G. Abdulaev and V. K. Aliev, Mater. Res. Bull. **15**, 1361 (1980).

[11]G. D. Guseinov, S. N. Mustafaeva, R. G. Guseinova, and E. G. Abdullaev, Phys. Status Solidi A **95**, K159 (1986).

[12]See, for instance, W. Heywang, *Amorphe und Polycrystalline Halbleiter* (Springer, Berlin, 1984), pp. 48–51.

[13]V. I. Tagirov, A. E. Bakhyshov, S. R. Samedov, L. G. Gasanova, and Khun Tkhikha, Fiz. Tekh. Poluprovodn. **14**, 1059 (1980) [Sov. Phys.—Semicond. **14**, 631 (1980)].

[14]G. D. Guseinov, G. D. Abdullaev, G. B. Bidzinova, S. M. Seidov, F. M. Ismailov, and M. Z. Pashyayev, Phys. Lett. **A33**, 421 (1970).

[15]K. Seeger, *Semiconductor Physics* (Springer, Berlin, 1985), pp. 40–42.

[16]F. Stöckman, Phys. Status Solidi A **64**, 475 (1981).

[17]A. N. Anagnostopoulos, Physica B (to be published).

[18]G. C. Vezzoli and I. H. Pratt, Thin Solid Films **14**, 161 (1972).

[19]G. C. Vezzoli, P. J. Walsh, and L. W. Doremus, J. Non-Cryst. Solids **18**, 333 (1975).

[20]K. W. Boer and S. R. Ovshinsky, J. Appl. Phys. **41**, 2675 (1970).

[21]R. M. Mehra, R. Shyam, and P. C. Mathur, J. Non-Cryst. Solids **31**, 435 (1979).

[22]D. M. Kroll, Phys. Rev. B **9**, 1669 (1974).

[23]M. Wolf and K. H. Müller, Phys. Status Solidi A **31**, K13 (1975).

[24]A. Abdel-A. Al., A. Elshajie, M. M. El Zaidia, and A. A. Ammar, Physica B **154**, 105 (1988).

[25]H. Hirashima, Y. Watanabe, and T. Yoshida, J. Non-Cry. Solids **95&96**, 825 (1987).